


5-1996

## Macrosegregation During Dendritic Arrayed Growth of Hypoeutectic Pb-Sn Alloys: Influence of Primary Arm Spacing and Mushy Zone Length

Surendra N. Tewari  
*Cleveland State University*

Rajesh Shah  
*Agmet Metals Inc.*

Follow this and additional works at: [https://engagedscholarship.csuohio.edu/encbe\\_facpub](https://engagedscholarship.csuohio.edu/encbe_facpub)

 Part of the [Materials Science and Engineering Commons](#)  
**How does access to this work benefit you? Let us know!**

### Original Citation

Tewari, S.N., & Shah, R. (1996). Macrosegregation During Dendritic Arrayed Growth of Hypoeutectic Pb-Sn Alloys: Influence of Primary Arm Spacing and Mushy Zone Length. *Metallurgical and Materials Transactions A: Physical Metallurgy and Materials Science* 27, 1353-1362.

### Repository Citation

Tewari, Surendra N. and Shah, Rajesh, "Macrosegregation During Dendritic Arrayed Growth of Hypoeutectic Pb-Sn Alloys: Influence of Primary Arm Spacing and Mushy Zone Length" (1996). *Chemical & Biomedical Engineering Faculty Publications*. 22.  
[https://engagedscholarship.csuohio.edu/encbe\\_facpub/22](https://engagedscholarship.csuohio.edu/encbe_facpub/22)

This Article is brought to you for free and open access by the Chemical & Biomedical Engineering Department at EngagedScholarship@CSU. It has been accepted for inclusion in Chemical & Biomedical Engineering Faculty Publications by an authorized administrator of EngagedScholarship@CSU. For more information, please contact [library.es@csuohio.edu](mailto:library.es@csuohio.edu).

# Macroseggregation During Dendritic Arrayed Growth of Hypoeutectic Pb-Sn Alloys: Influence of Primary Arm Spacing and Mushy Zone Length

S.N. TEWARI and R. SHAH

Thermosolutal convection in the dendritic mushy zone occurs during directional solidification of hypoeutectic lead tin alloys in a positive thermal gradient, with the melt on the top and the solid below. This results in macrosegregation along the length of the solidified samples. The extent of macrosegregation increases with increasing primary dendrite spacings for constant mushy zone length. For constant primary spacings, the macrosegregation increases with decreasing mushy zone length. Presence of convection reduces the primary dendrite spacings. However, convection in the interdendritic melt has significantly more influence on the spacings as compared with that in the overlying melt, which is caused by the solutal buildup at the dendrite tips.

## I. INTRODUCTION

**MACROSEGREGATION** during dendritic growth of alloys is a serious concern for all the casting processes. It is caused by the combined effects of sedimentation or floating of equiaxed grains or dendrite fragments and convection in the interdendritic melt. Convection is caused by thermal and solutal instabilities and also by the solidification shrinkage (advection). Sedimentation and thermal convection effects can be eliminated by a suitable selection of the alloy composition and growth conditions during directional solidification. However, terrestrial experiments do not allow us to isolate the advection from the thermosolutal convection effects for a systematic study of their influence on the macrosegregation. Low gravity experiments would be required for this purpose. In order to identify the optimum growth conditions for such a potential study, we have been examining macrosegregation in hypoeutectic Pb-Sn alloys, directionally solidified in a positive thermal gradient, the melt on the top and the solid below. Under such growth conditions, the temperature profile alone is expected to be stabilizing against natural convection. However, the interdendritic solutal profile is destabilizing because the tin content of the mushy zone melt decreases from  $C_E$  (eutectic composition) at the base of the array to  $C_t$  at the dendrite tip. For the dendritic morphology,  $C_t$  is only slightly more than the solute content of the bulk alloy,  $C_0$ . Thus, the tin poor higher density melt is on top and the tin rich low density melt is at the bottom of the mushy zone. The intensity of the resulting interdendritic convection, and hence the extent of the macrosegregation along the length of the directionally solidified specimens, is expected to depend on  $C_0$  and the mushy zone morphology (the primary dendrite spacings ( $\lambda_1$ ) and the length of the mushy zone ( $H$ )). It has been observed that the macrosegregation shows a maximum

with  $C_0$ ; zero macrosegregation for 10 and 58 wt pct Sn and maximum for 33 wt pct Sn.<sup>[1]</sup> The solutal buildup at the tips of the dendrite array ( $C_t - C_0$ ) which increases with increasing  $G_t/R$  (where  $G_t$  is the thermal gradient in the liquid at the array tips and  $R$  is the growth speed) produces an unstable density profile in the overlying melt, immediately ahead of the array. The resulting convection produces extensive longitudinal macrosegregation, especially for the samples grown with a cellular morphology.<sup>[2]</sup> It has been observed that the application of transverse magnetic field, up to about 0.45  $T$ , during directional solidification has no influence on the macrosegregation, whether the convection was due to the density inversion in the interdendritic melt or in the overlying melt, immediately ahead of the mushy zone.<sup>[3]</sup>

In this article, we will examine the influence of primary dendrite spacings and the mushy zone length on the longitudinal macrosegregation due to the interdendritic convection during directional solidification of hypoeutectic Pb-Sn alloys. We will also compare the experimentally observed primary dendrite spacings with those expected from the theoretical models, which assume diffusive thermal and solutal transports, in order to understand the effect of natural convection on the primary dendrite spacings.

## II. EXPERIMENTAL PROCEDURE

About 24- to 30-cm-long Pb-Sn feedstock samples were obtained by induction melting a charge (lead and tin, 99.99 pct purity) under an argon atmosphere in a quartz crucible and pushing the melt into evacuated quartz tubes (0.7-cm i.d.) with the help of argon pressure. The quartz tubes contained either one or two Chromel-Alumel thermocouples (0.01-cm diameter wires kept within closed end quartz capillaries, 0.06-cm o.d.) which were located along the sample length with a longitudinal separation of about 2 cm. After sealing one end, the quartz tubes containing these samples were evacuated and the top 15- to 20-cm length of the cast specimen was remelted. Directional solidification was carried out by raising the furnace assembly at various growth speeds with respect to the stationary sample. The furnace and experimental details were presented ear-

S.N. TEWARI, Professor, is with the Chemical Engineering Department, Cleveland State University, Cleveland, OH 44115. R. SHAH, formerly Graduate Student, Chemical Engineering Department, Cleveland State University, is Research Engineer, Agmet Metals Inc., Oakwood Village, OH 44146.

Manuscript submitted December 29, 1994.

**Table I. Experimental and Morphological Details of Directionally Solidified Pb-Sn Alloys**

Specimen	$C_0$ (Wt Pct Sn)	$R$ ( $\mu\text{m s}^{-1}$ )	$G$ (K $\text{cm}^{-1}$ )	$\lambda_1$ ( $\mu\text{m}$ )	$R_H$ ( $\mu\text{m}$ )	$H_F$ (cm)	$f_E$	Freckles (Number, Location)	$(C_{FS=0.6} - C_{FS=0.2})$ (Wt Pct Sn)
4a	33.4	8	75	166	9.2	0.77	0.40	2 (out)	4.33
4c	34.0	30	17	172	8.4	2.80	0.34	1 (out)	2.31
3b	23.7	24	81	164	6.0	1.45	0.19	0	3.61
3c	23.4	6	77	185	6.3	1.28	0.16	2 to 3 (out)	3.21
3d	27.0	64	59	155	7.2	1.51	0.33	0	2.26
3f	30.3	6	20	208	10.0	1.90	0.36	1 (in)	6.45
3g	27.1	1	17	240	—	1.89	—	1 (in)	18.6
SN001	10.0	10	110	115	—	—	0.01	0	0.07
1a	16.5	4	101	172	5.9	1.66	0.09	1 (out)	1.1
5a	57.9	10	105	234	249.3	0.051	0.93	0	0
5b	54.7	40	67	177	21.3	0.106	0.84	0	0.2

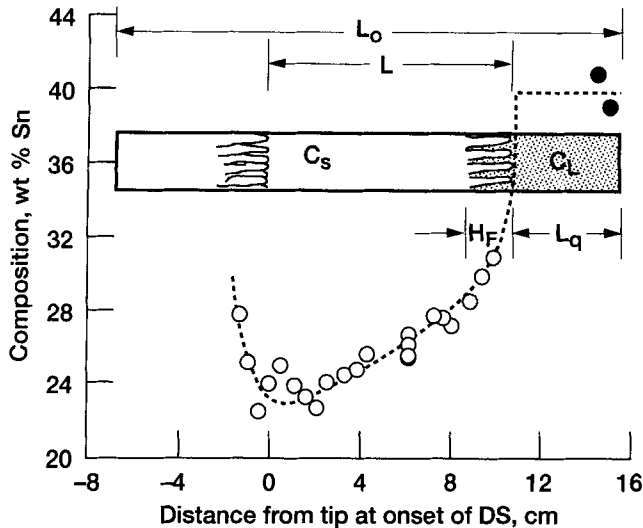


Fig. 1—Typical macrosegregation along the length of the directionally solidified and quenched specimen. The open symbols represent the directionally solidified portion. The closed symbols represent the quenched liquid portion. ( $C_0 = 30.3$  pct Sn,  $R = 6 \mu\text{m s}^{-1}$ ,  $G = 20 \text{ K cm}^{-1}$ , specimen 3f). The schematic drawing shows the initial and final locations and lengths of the mushy zone.

lier.<sup>[1-4]</sup> The growth was vertically upward, and a steady-state thermal profile was maintained as indicated by identical thermal profiles obtained from the two thermocouples.<sup>[4]</sup> After 10 to 14 cm of directional growth, the specimens were quenched by directing a jet of helium gas, cooled by liquid nitrogen, to the surface of the quartz crucibles. The furnace translation rate was equal to the directional solidification speed; this was verified by correlating the longitudinal (parallel to the growth direction) microstructure of the directionally solidified specimen with the furnace translation distance.

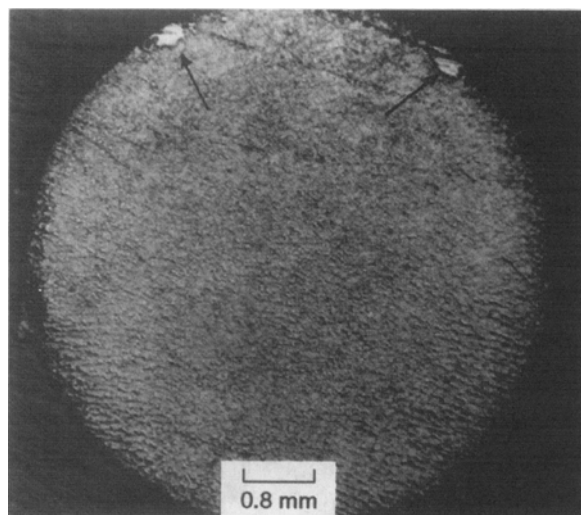
Longitudinal and transverse microstructures were examined in the unetched condition by standard optical metallography techniques. Transverse microstructures were also quantitatively analyzed to obtain the average primary dendrite spacing ( $\lambda_1$ ), dendrite perimeter, and area fraction of the interdendritic eutectic ( $f_E$ ) at the base of the mushy zone, with the help of image analysis software.<sup>[5]</sup> Hydraulic radius ( $R_H$ ), defined as the ratio of the dendrite perimeter and the cross-sectional area occupied by the interdendritic eutectic, was also measured. Atomic absorption spectrometry was used to determine the tin contents of thin slices ( $\approx 0.3$ -cm

thick), cut along the length of the directionally solidified and quenched portion of the specimen. The ratio of the distance solidified, as measured from the tip of the mushy zone at the onset of directional solidification, to the total length of the initial melt column was taken as the fraction solidified ( $f_s$ ). Table I lists the growth parameters for all the specimens examined in this study.

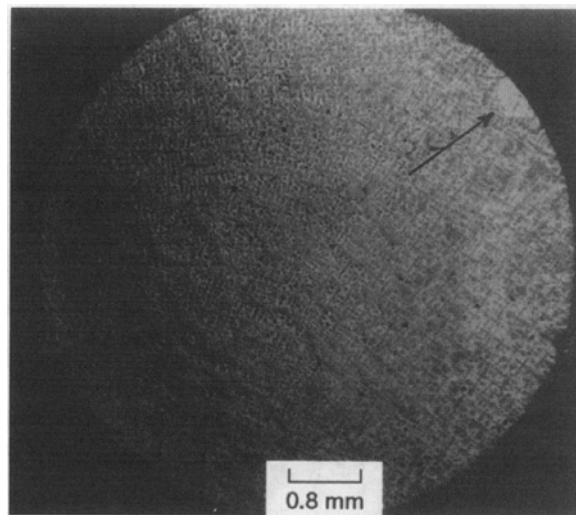
### III. RESULTS

Figure 1 shows a typical specimen configuration during directional solidification and quenching process and the resulting longitudinal macrosegregation. The initial length of the precast specimen is  $L_0$ . The length of the liquid column, ahead of the dendrite array tips, at the time of quench is  $L_q$ . It is assumed that at the onset of directional solidification, the dendrite tips are located at a distance equal to the total furnace translation distance ( $L$ ) away from their location at the time of quench. As mentioned earlier, the fraction solidified ( $f_s$ ) is defined as the ratio of the solidification distance to the length of the initial melt column, both measured from the location of the array tips at the onset of directional solidification. The symbol,  $C_s$ , denotes the tin content of the 0.3-cm-thick slice at any  $f_s$ . The composition of the quenched liquid portion of the specimen is denoted by  $C_L$ . The length of the mushy zone at the time of quench ( $H_F$ ), assumed to be equal to the distance between the liquidus temperature corresponding to  $C_L$  and the eutectic temperature, is also indicated in this figure.

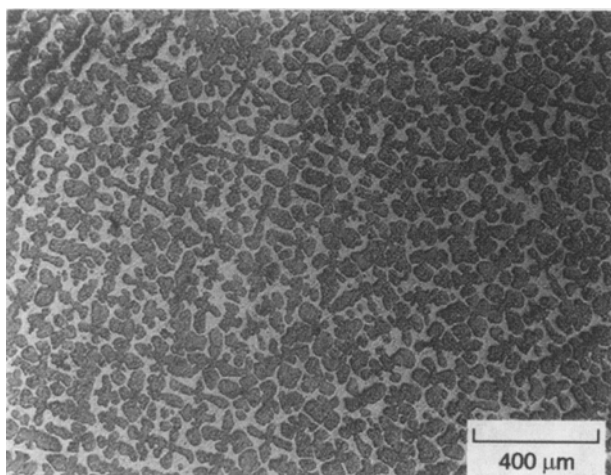
The typical macrosegregation along the length of a directionally solidified specimen is also shown in Figure 1. Here, the open symbols denote the tin content in the directionally solidified portion, and the filled symbols denote the tin content in the quenched melt portion. The initial decrease in the tin content in the directionally solidified specimen corresponds to the region where the two phases, liquid + solid, existed during the remelting of the precast feedstock prior to the onset of directional solidification. Microstructural examination showed that the aligned dendrite arrays developed only after the growth had occurred for a distance approximately equal to one mushy zone length. When the directional solidification begins, the shrinkage driven flow brings in the solute poor melt from near the top of the solid plus liquid region toward its bottom. This flow must be responsible for the observed initial decrease in the tin content shown in Figure 1. However, it should



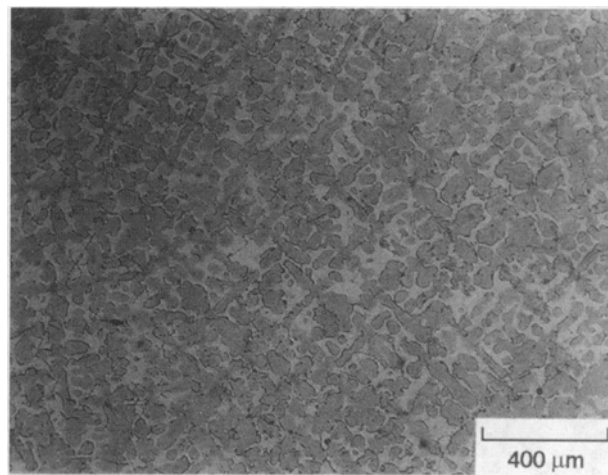
(a)



(b)



(c)



(d)

Fig. 2—Transverse microstructures of the directionally solidified Pb  $\approx$ 33 wt pct Sn alloys. (a) Low and high magnification views;  $G_i = 75 \text{ K cm}^{-1}$ ,  $R = 8 \text{ } \mu\text{m s}^{-1}$  (specimen 4a). (b) Low and high magnification views;  $G_i = 17 \text{ K cm}^{-1}$ ,  $R = 30 \text{ } \mu\text{m s}^{-1}$  (specimen 4c).

be noted that such decrease could only be observed for specimens with the mushy zone significantly longer than 0.3 cm. (The thickness of the disks used for the atomic absorption spectrometry is about 0.3 cm.)

Subsequent growth of the mushy zone causes thermosolutal convection which is responsible<sup>[1]</sup> for the positive segregation of tin, indicated in Figure 1. Initial solute contents ( $C_0$ ) obtained by measuring the areas under the  $C_s$  vs  $f_s$  curves were within  $\pm 5$  pct of the analyses of the precast feedstock alloy. It has been previously observed<sup>[4]</sup> that steady-state thermal profiles are maintained during growth of these specimens. The increasing tin content of the melt is expected to reduce the mushy zone length and increase the primary dendrite spacings along the specimen length. It would have been ideal to vary only one parameter, *e.g.*, mushy zone length, and measure the longitudinal macrosegregation, while keeping constant all the other parameters, such as primary dendrite spacings, thermal and composition gradients, volume fraction eutectic, *etc.* However, such experiments are not possible. Therefore, in the following sections, we will assume that the mushy zone morphologies at the time of quench ( $\lambda_1$  and  $H_F$ ) represent

the overall growth conditions in order to obtain a qualitative understanding of their relationship with natural convection.

#### A. Influence of Mushy Zone Length

Let us examine two specimens, 4a and 4c (Table I), which were grown with nearly identical compositions (33.4 and 34.0 wt pct Sn), primary dendrite spacings (166 and 172  $\mu\text{m}$ ), volume fraction of eutectics at the base of dendrites ( $f_E$ ) (0.40 and 0.34), and hydraulic radii at the base of dendrites (9.2 and 8.4  $\mu\text{m}$ ), but with significantly different mushy zone lengths ( $H_F = 0.77$  and 2.80 cm). Specimens 4a and 4c were, respectively, grown at  $8 \text{ } \mu\text{m s}^{-1}$  with  $G_i = 75 \text{ K cm}^{-1}$  and at  $30 \text{ } \mu\text{m s}^{-1}$  with  $G_i = 17 \text{ K cm}^{-1}$ . Figure 2 shows transverse microstructures from these specimens. The lower magnification views are of the entire cross sections, and the higher magnification views show the primary dendrites. Their microstructures are similar. The primary dendrites are uniformly distributed across the entire specimen cross section, except for the small tin-rich freckles indicated by the arrows. There are two freckles in Figure

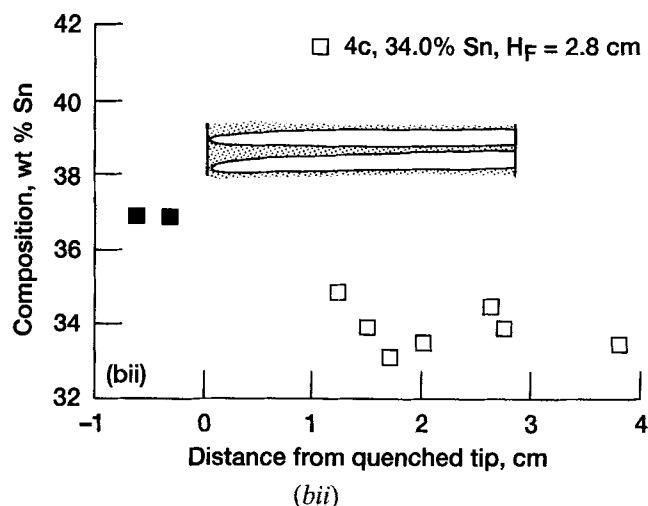
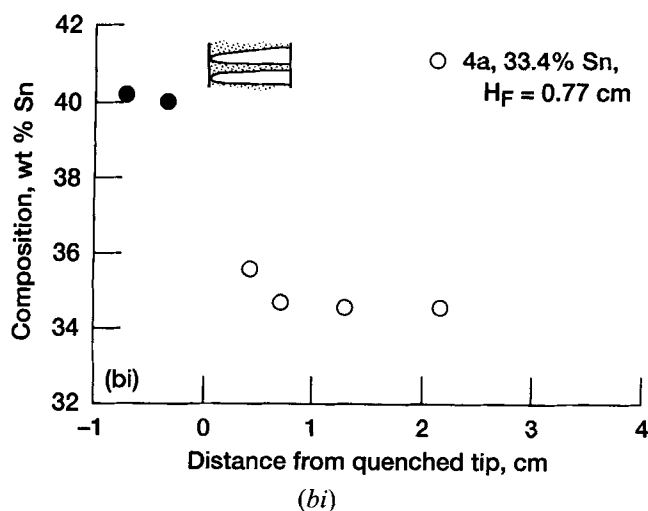
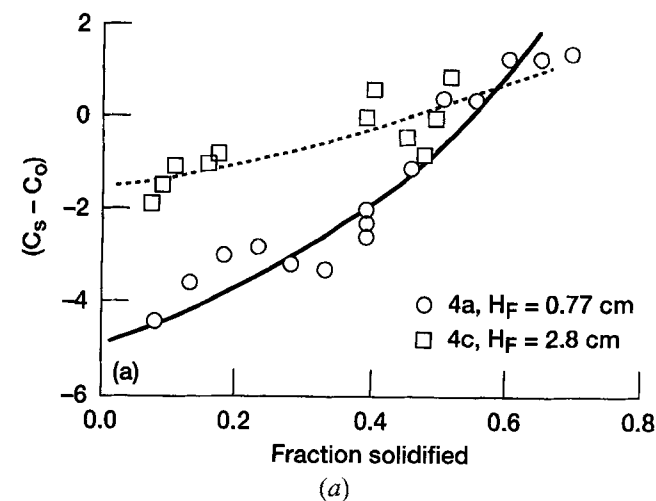


Fig. 3—Influence of the mushy zone length on the longitudinal macrosegregation for constant primary dendrite spacings (specimen 4a:  $C_0 = 33.4$  at. pct Sn,  $\lambda_1 = 166 \mu\text{m}$ ,  $H_F = 0.77$  cm; and specimen 4c:  $C_0 = 34.0$  at. pct Sn,  $\lambda_1 = 172 \mu\text{m}$ ,  $H_F = 2.80$  cm). (a) Macrosegregation along the length of the directionally solidified specimens. (b) Macrosegregation profiles within the quenched mushy zone: (i) specimen 4a and (ii) specimen 4c.

2(a) and one in Figure 2(b); all are located at the crucible wall.

Figure 3(a) is a plot of  $(C_s - C_0)$  vs fraction solidified for specimens 4a and 4c. For an improved clarity of presentation, the data from the quenched liquid portions of the specimen are not included in Figure 3(a); only the data from the directionally solidified portions are included. Specimen 4c, grown with the larger mushy zone length ( $H_F = 2.8$  cm), has less longitudinal macrosegregation than specimen 4a ( $H_F = 0.77$  cm). This observation suggests that a longer mushy zone would reduce the extent of thermosolutal convection.

The preceding observation is further confirmed by examining the solute content in the quenched mushy region of the two specimens, shown in Figures 3b(i) and b(ii). Locations of the mushy zone at the time of quench are also indicated in these figures. The filled symbols represent the quenched melt portion ahead of the array tips. The open symbols represent the tin content in the directionally solidified portion and also the average tin content of the solid plus interdendritic liquid in the mushy region. The composition in the directionally solidified portion, the average solid plus liquid composition in the quenched mushy zone, and the composition in the quenched melt would be expected to be identical for a diffusive solutal transport. In addition, one would expect the variation of tin content in both specimens to be identical in the absence of convection. Thermosolutal convection, however, has caused the average solute content of the mushy region to rise from the base of the dendrites toward their tips, with most of the buildup confined to the top 30 pct of the mushy zone. This solutal buildup is greater for the specimen with the smaller mushy zone length, 4a (from 34.8 to 40.2 wt pct Sn) compared to specimen 4c (from 33.8 to 36.8 wt pct Sn).

## B. Influence of Primary Dendrite Spacing

### 1. Freckles

Figures 4(a) through (d) show low magnification, transverse views of the specimens studied for examining the influence of primary dendrite spacings on the longitudinal macrosegregation. These sections are from the directionally solidified portions, in the immediate vicinity of the quenched mushy zone. These alloys were of similar composition,  $C_0 = 26.9 \pm 3.4$  wt pct tin. Their mushy zone lengths at the time of quench ( $H_F$ ) were also approximately similar, varying from 1.28 to 1.90 cm. Other details of the growth conditions and microstructures are presented in Table I. There was a systematic variation in their primary dendrite spacings, with 3d (155  $\mu\text{m}$ ), 3b (164  $\mu\text{m}$ ), 3c (185  $\mu\text{m}$ ), 3f (208  $\mu\text{m}$ ), and 3g (240  $\mu\text{m}$ ). Distributions of primary dendrites were uniform across the specimens, except for the tin-rich freckles, which are marked by arrows in Figure 4. The specimens with the smallest primary dendrite spacings (3d and 3b) did not contain freckles (Figures 4(a) and (b)). Specimen 3c contained two freckles, which were located at the crucible wall (Figure 4(c)). The specimens 3f with larger primary dendrite spacings showed freckles in the interior of the specimen (Figure 4(d)). The specimen 3g (figure not shown here) also showed one freckle which was located in the interior of the specimen. It was observed that the number of surface freckles remained constant, and their relative position did not change much during directional solidification. In contrast, two internal freckles formed in

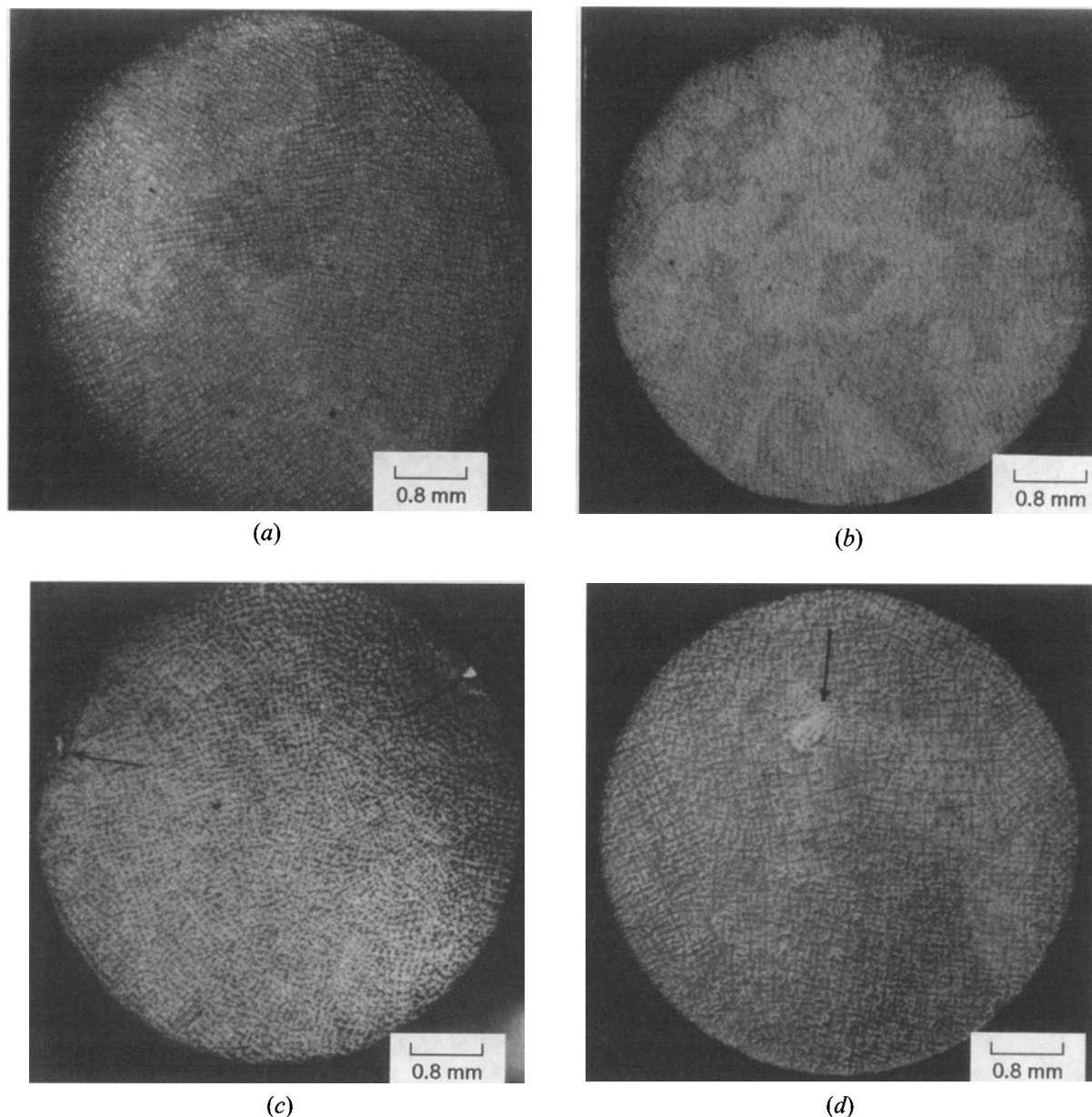


Fig. 4—Transverse microstructures of the Pb-26.9  $\pm$  3.4 wt pct Sn alloy, directionally solidified to yield increasing primary dendrite spacings. Growth conditions are given in Table I (a) Specimen 3d:  $\lambda_1 = 155 \mu\text{m}$ ; (b) specimen 3b:  $\lambda_1 = 164 \mu\text{m}$ ; (c) specimen 3c:  $\lambda_1 = 185 \mu\text{m}$ ; and (d) specimen 3f:  $\lambda_1 = 208 \mu\text{m}$ .

specimens 3f and 3g in the beginning, and they merged to one freckle for the remainder of the directionally solidified length.

It has been suggested that the location of the channel segregates depends on the macroscopic shape of the liquid-solid interface near the tips of the dendrite array. The channels form in the interior of the specimen for the interfaces which are concave toward the melt. They form on the exterior surface for the convex interfaces. Examination of the longitudinal microstructures at the quenched liquid-solid interfaces did not reveal any such curvature in these specimens. In a previous study on Pb-Sn alloys with larger diameters<sup>[6]</sup> (3.8 vs 0.7 cm in this study) and larger primary arm spacings (280 to 380 vs 150 to 240  $\mu\text{m}$  in this study), the freckles were located in the interiors. It appears from this study that the location of the freckles, whether in the

interior or on the outer periphery, is determined by the primary dendrite spacings. Larger primary dendrite spacings favor freckles in the interior, but a more systematic study with various mold diameters and primary arm spacings would be required to confirm this observation.

## 2. Macrosegregation

Figure 5(a) shows the influence of primary dendrite spacings on the extent of longitudinal macrosegregation for alloys with approximately similar compositions ( $C_0 = 26.9 \pm 3.4$  wt pct tin). Data from the initial transient portion (fraction solid  $< 0.2$ ) and quenched liquid portion have not been included in this figure for the sake of clarity of presentation. Multiple data at a given  $f_s$  represent the variation in the tin content in the radial direction. Chips obtained by machining the specimen in a lathe were used to obtain these

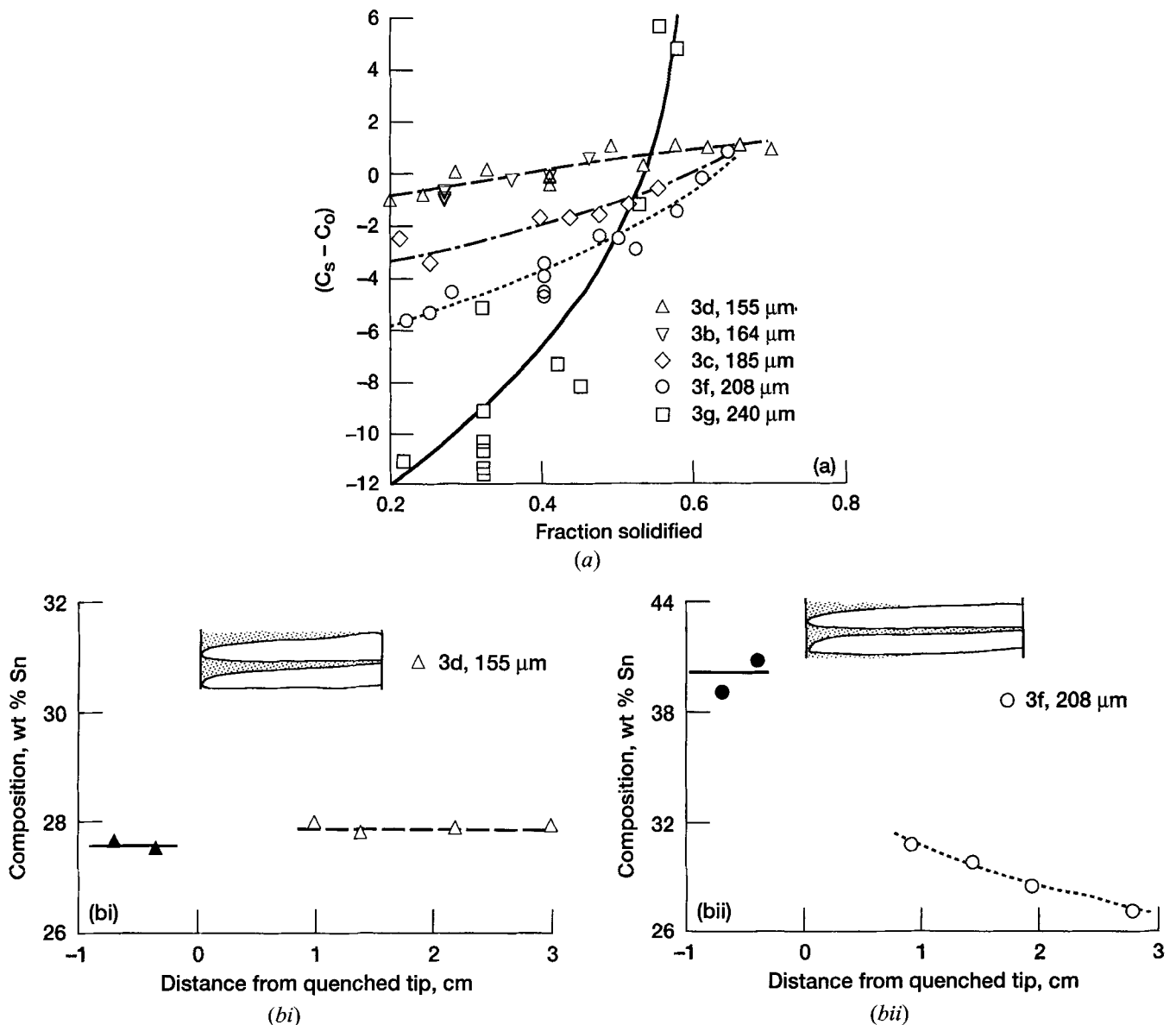


Fig. 5—Effect of primary dendrite spacings on the longitudinal macrosegregation for nearly constant mushy zone lengths (specimen 3d:  $C_0 = 27.0$  at. pct Sn,  $H_F = 1.51$  cm; specimen 3b:  $C_0 = 23.7$  at. pct Sn,  $H_F = 1.45$  cm; specimen 3c:  $C_0 = 23.4$  at. pct Sn,  $H_F = 1.90$  cm; and specimen 3g:  $C_0 = 27.1$  at. pct Sn,  $H_F = 1.89$  cm). The primary dendrite spacings are indicated in the figures. (a) Macrosegregation along the length of the directionally solidified specimens. (b) Macrosegregation profiles within the quenched mushy zone (open symbols). Filled symbols indicate the composition of the melt at the time of quench. The mushy zones at the time of quench are indicated schematically. (i) specimen 3d ( $\lambda_1 = 155 \mu\text{m}$ ) and (ii) specimen 3f ( $\lambda_1 = 208 \mu\text{m}$ ).

data. Specimens 3d ( $\lambda_1 = 155 \mu\text{m}$ ) and 3b ( $\lambda_1 = 164 \mu\text{m}$ ), with nearly identical macrosegregation profiles, show the least amount of longitudinal macrosegregation. Macrosegregation increases as the primary arm spacings increase from 164 to 240  $\mu\text{m}$ . The extent of macrosegregation is also associated with the presence of freckles and their sizes. Specimens 3d and 3b, with no freckles (Figures 4(a) and (b)), showed little longitudinal macrosegregation. Specimen 3c, with two small surface freckles (Figure 4(c)), showed more macrosegregation. Specimens 3f and 3g, with one relatively large internal freckle (Figure 4(d)), showed the maximum macrosegregation.

Figures 5b(i) and b(ii) show the influence of increasing primary arm spacings on the solutal profiles in the

quenched mushy zone. The filled symbols represent the quenched melt portion ahead of the array tips. The open symbols represent the tin content in the directionally solidified portion and also the average tin content of the solid plus interdendritic liquid in the mushy region. Similar to the behavior described earlier (Figures 4b(i) and b(ii)), the compositions of the directionally solidified portion, of the mushy region, and of the quenched melt portion are nearly identical for specimen 3d, in which very little longitudinal macrosegregation was observed (Figure 5(a)). On the other hand, there is a large solute buildup in the mushy region of specimen 3f, which showed extensive longitudinal macrosegregation (Figure 5(a)). As shown in Figure 5b(ii), the tin content for this specimen increased

from 28.4 wt pct at the base of the dendrites to 40.4 wt pct near the array tips.

#### IV. DISCUSSION

##### A. Solutal Rayleigh Number and Characteristic Length Scale

Onset of thermosolutal convection and its influence on solutal redistribution has been extensively investigated for directional solidification of binary alloys with a planar liquid-solid interface.<sup>[7,8]</sup> However, these phenomena for dendritic microstructures are not as well understood. Since the morphology of the mushy zone (interdendritic volume fraction liquid and permeability) and the interdendritic convection are coupled with each other (each affects the other), an accurate numerical analysis of the phenomena has not been possible. Poirier and co-workers<sup>[9]</sup> have recently attempted to analyze this process by using the well-known nondimensional fluid mechanics parameters. Some of these parameters, such as the Prandtl and Schmidt numbers, are determined solely by the alloy physical properties. Whereas others, such as thermal and solutal Rayleigh and Darcy numbers, are dependent upon the growth conditions and the mushy zone morphology. The thermal and solutal Rayleigh numbers, defined as  $Ra_T = g\alpha \Delta TH^3/K_l\nu$  and  $Ra_s = g\beta\Delta CH^3/D_l\nu$ , are generally used to describe the onset of convection in the melt.<sup>[6,8,9]</sup> Here,  $\alpha$  and  $\beta$  are the thermal and solutal coefficients of volumetric expansion,  $K_l$  and  $D_l$  are the thermal and solutal diffusivities, and  $\nu$  is the kinematic viscosity of the melt. The temperature and composition differences which drive the convection are  $\Delta T$  and  $\Delta C$ . The other parameters are  $g$ , the acceleration due to gravity, and  $H$ , the characteristic length scale. For a planar liquid-solid interface,  $D_l/R$  has been assumed to represent the characteristic length,<sup>[10]</sup> where  $R$  is the growth speed. However, for the dendritic arrays, there are three length scales which may be used as the characteristic length, the ampoule diameter ( $d$ ), the mushy zone length, as used in Reference 9, and the primary dendrite spacing ( $\lambda_1$ ), as used in Reference 6. Which one is the most appropriate to describe the interdendritic thermosolutal convection? As shown by Duval,<sup>[11]</sup> identification of the proper length scale in the Rayleigh number is very important in order to accurately predict the onset of the natural convection in a contained fluid column. In case the characteristic length is not properly selected, contrary to the usual expectation, the increasing Rayleigh number may not yield more instability, *i.e.*, more intensive convection.

For our experiments, we can use  $\Delta T$  and  $\Delta C$  to be, respectively, the temperature and composition differences between the tip and the base of the mushy zone. Use of the physical properties for the Pb-Sn alloys,  $\alpha = 1.15 \times 10^{-4} \text{ K}^{-1}$ ,  $K = 1.08 \times 10^{-5} \text{ m}^2 \text{ s}^{-1}$ ,  $\nu = 2.47 \times 10^{-7} \text{ m}^2 \text{ s}^{-1}$ ,  $\beta = 5.2 \times 10^{-3} \text{ wt pct}^{-1}$ ,  $D_l = 3 \times 10^{-9} \text{ m}^2 \text{ s}^{-1}$ , yields the thermal and solutal Rayleigh numbers to be  $4 \times 10^8 (\Delta T)H^3$  and  $7 \times 10^{13} (\Delta C)H^3$  (the Pb-Sn properties have been taken from Reference 6). Since  $Ra_s$  is several orders of magnitude larger than  $Ra_T$ , we will examine our macrosegregation data with respect to  $Ra_s$ . Figure 6 plots the extent of longitudinal macrosegregation vs  $Ra_s$  in order to identify the most appropriate length scale,  $H$ . Data from Table I and from Ref-

erence 1 (specimens SN001, 1a, 5a, and 5b) have been used in Figure 6. Here, the extent of the macrosegregation has been defined as the difference between the compositions at fraction solid ( $f_s$ ) equal to 0.60 and 0.20. The crucible diameter ( $d$ ), the mushy zone length ( $H_F$ ), and the primary dendrite spacings ( $\lambda_1$ ) have been used as  $H$  to obtain the corresponding solutal Rayleigh numbers,  $R_{sd}$  (Figure 6(a)),  $R_{sH}$  (Figure 6(b)), and  $R_{s\lambda}$  (Figure 6(c)). Use of crucible diameter (Figure 6(a)) and mushy zone length (Figure 6(b)) does not yield any correlation between the extent of the longitudinal macrosegregation and solutal Rayleigh number. Only the use of the primary dendrite spacing as the characteristic length (Figure 6(c)) yields the expected behavior, *i.e.*, increasing solutal Rayleigh number resulting in an increased longitudinal macrosegregation due to more intense interdendritic convection. This suggests that the appropriate length scale to describe convection in the mushy zone is the primary dendrite spacings.

##### B. Influence of Convection on Primary Dendrite Spacings

Analytical<sup>[12-15]</sup> and numerical<sup>[16]</sup> models have been proposed in the literature to predict the dependence of primary dendrite spacings on growth speed, thermal gradient, and alloy composition. Hunt<sup>[12]</sup> proposed the following analytical relationship to predict the primary dendrite spacings,  $\lambda_1$ :

$$(\lambda_1)^2 = 4\sqrt{2} [(G_c/G_c) - 1] (D_l/R) r_i \quad [1]$$

where  $G_c$  is the solutal gradient in the melt at the dendrite tips,  $G_c$  is the solutal gradient in the interdendritic melt, and  $r_i$  is the dendrite tip radius. Several approaches have been taken to obtain the tip radius value required in relationship, [1] *e.g.*, assumption of minimum undercooled dendrite tip,<sup>[12,13]</sup> assumption of paraboloidal dendrite tip shape coupled with the tip stability criterion,<sup>[14]</sup> and assumption of ellipsoidal dendrite tip shape coupled with the marginal stability criterion.<sup>[15]</sup> All these models assume diffusive thermal and solutal transport and do not take convection into account. Since convection is expected to influence the solutal profiles at the tip and also the composition gradient in the interdendritic melt, the primary dendrite spacings are expected to be influenced by convection. The convection would also influence the tip radius and, hence, the primary dendrite spacings. However, it is not apparent as to which one of these two convective flows, the one in the interdendritic mushy region or that in the melt immediately ahead of the dendrite tips, has a more dominant influence on the primary dendrite spacings. Even though the two fluid flows are coupled, it is possible to examine their effects separately by comparing the experimentally observed primary dendrite spacings with those predicted from the theoretical models. In the following, we will use the model due to Hunt.<sup>[12]</sup> (We will use the effective thermal gradient,  $G_l$ <sup>[17]</sup> instead of  $G_i$  to account for the different solid and liquid thermal conductivities and the heat of fusion.) This model assumes minimum undercooling at the dendrite tips to obtain the dendrite tip radius and includes the interaction between the neighboring dendrites in its analysis. However, the purpose here is not to examine the validity of the various theoretical models, but to compare the primary dendrite spacings ob-

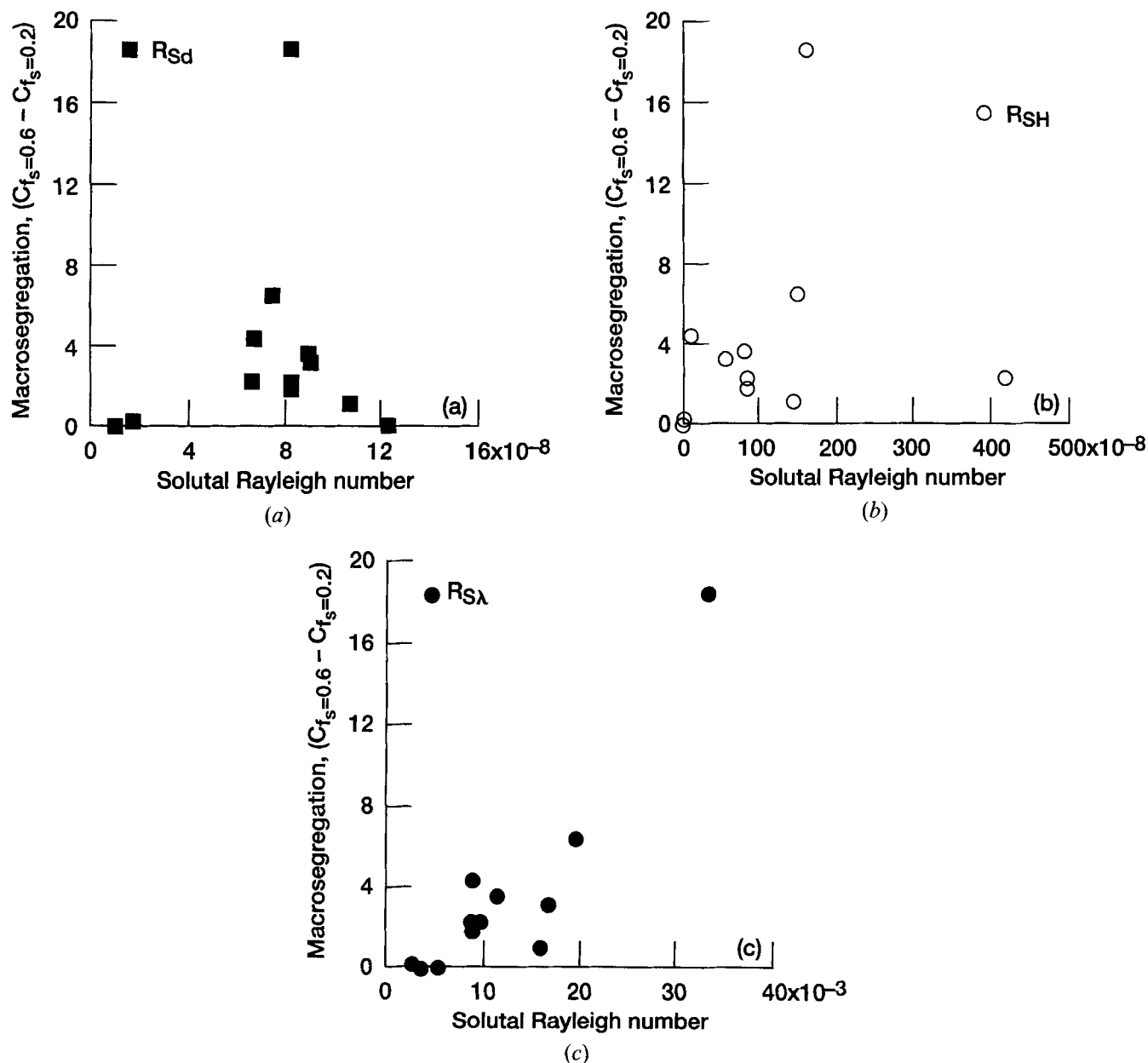


Fig. 6—Dependence of the longitudinal macrosegregation on the solutal Rayleigh numbers, based on the characteristic length ( $H$ ) being equal to (a) crucible diameter, (b) mushy zone length, and (c) primary dendrite spacings.

served under increasingly convective growth conditions with those expected in the absence of convection.

#### 1. Convection due to solutal buildup at the dendrite tips

It has been shown earlier<sup>[2]</sup> that directionally solidified Pb-10 wt pct Sn specimens grown at  $110 \text{ K cm}^{-1}$  and  $10 \mu\text{m s}^{-1}$  do not show any longitudinal macrosegregation, suggesting minimal interdendritic convection. However, as the growth speed was decreased, the extent of longitudinal macrosegregation increased due to the convection caused by the solutal buildup in the melt ahead of the dendrite tips.<sup>[2]</sup> Since increased tin content results in reduced melt density, the solutal buildup causes convection in the melt ahead of the dendrite tips, which results in an increased longitudinal macrosegregation. For a diffusive solutal transport, the solutal buildup  $(C_1 - C_0)$  increases with the increasing value of  $D_l G / R \Delta T_0$ ,<sup>[13-16]</sup> where  $\Delta T_0$  is the alloy

freezing range. The parameter  $D_l G / R \Delta T_0$ , therefore, can be used to represent the extent of convection caused by the solutal buildup at the tips. Figure 7(a) plots the ratio of the experimentally observed and the theoretically predicted primary dendrite spacings as a function of  $D_l G / R \Delta T_0$ . These data have been taken from Reference 4. (Only the dendritic morphology specimens from Reference 4 are included; the cellular morphology specimens are not included.) Figure 7(a) shows that at large growth speeds, low  $D_l G / R \Delta T_0$  value, there is an excellent agreement with the analytical model. However, there is a systematic decrease in the primary dendrite spacing ratio with the increasing  $D_l G / R \Delta T_0$ . Increased convection ahead of the dendritic tips results in reduced primary dendrite spacings. Growth under the maximum solutal buildup (the morphology became cellular for  $D_l G / R \Delta T_0 > 0.34$ <sup>[4]</sup>) condition results in about 16 pct decrease in the arm spacings due to convection.

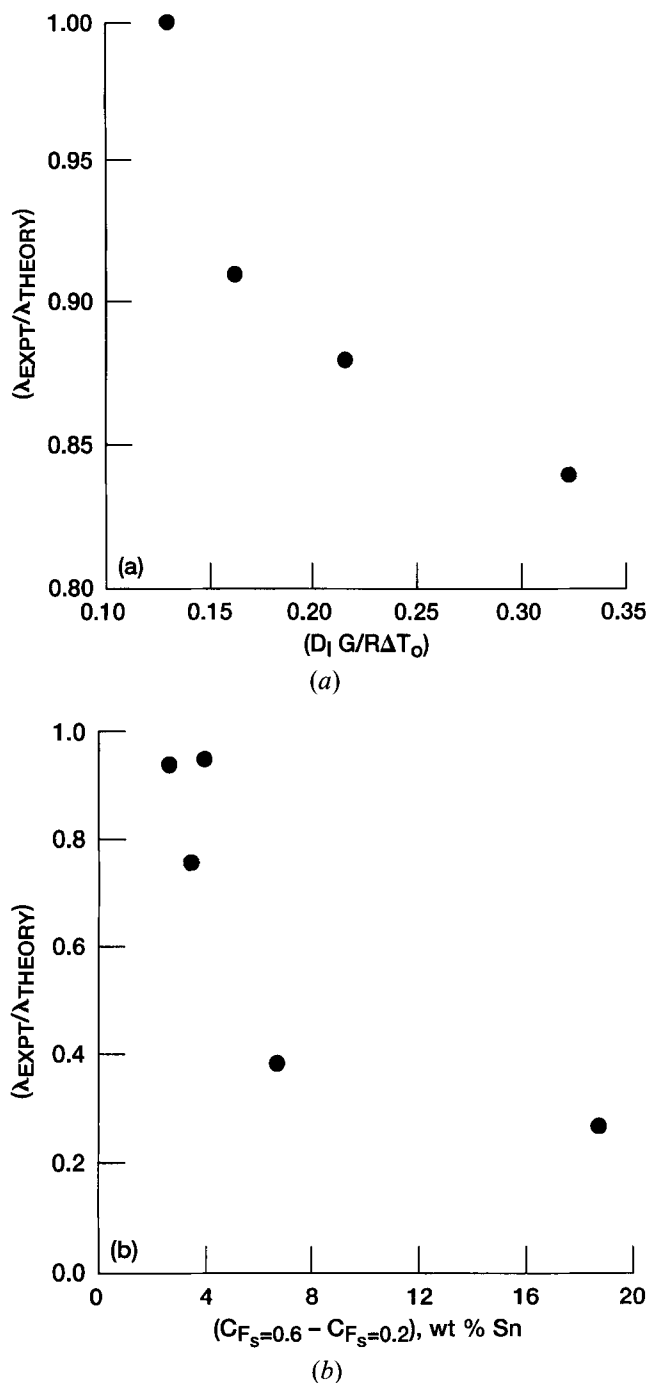


Fig. 7—Influence of convection on the primary dendrite spacings. (a) Ratio of the experimentally observed and theoretically predicted primary dendrite spacing vs  $D_l G / R \Delta T_0$ . (b) Ratio of the experimentally observed and theoretically predicted primary dendrite spacing vs extent of macrosegregation ( $C_{FS=0.6} - C_{FS=0.2}$ ).

## 2. Convection due to the interdendritic solutal profile

The specimens 3d, 3b, 3c, 3f, and 3g (Table I) were directionally solidified with  $D_l G / R \Delta T_0$  values which are much less than 0.04, i.e., insignificant solutal buildup at the dendrite tips. The longitudinal macrosegregation is therefore caused mainly by the interdendritic convection. Figure 7(b) plots the ratio of the experimentally observed and the theoretically predicted primary spacings as a function of  $(C_{FS=0.6} - C_{FS=0.2})$ , the extent of longitudinal macrosegregation. As mentioned earlier, the increasing  $(C_{FS=0.6} -$

$C_{FS=0.2})$  indicates larger intensity of the interdendritic convection. The primary dendrite spacings for small convection (small macrosegregation values) are about 95 pct of those predicted theoretically. However, there is a systematic decrease in the arm spacing ratio with increasing convection, represented by the larger values of  $(C_{FS=0.6} - C_{FS=0.2})$ . The growth condition with the highest  $(C_{FS=0.6} - C_{FS=0.2})$  value, i.e., the maximum convection, yields arm spacing which is only 30 pct of the theoretical predictions. For specimen 3g, the experimentally observed primary dendrite spacing is only 240  $\mu\text{m}$ , as compared with the theoretically predicted value of 869  $\mu\text{m}$ . The 869- $\mu\text{m}$  value is based on  $C_0 = 27.1$  wt pct tin, the overall solute content of the specimen. If we use the tin content of the quenched melt, 40.3 wt pct Sn, as the alloy composition, the predicted arm spacing would be even larger, about 962  $\mu\text{m}$ .

A comparison between Figures 7(a) and (b) suggests that for the dendritic morphologies, the interdendritic convection has significantly larger impact on the primary arm spacings as compared with that caused by the solutal buildup. This observation is in agreement with a recent low gravity experiment,<sup>[18]</sup> where primary arm spacings were observed to be about 4 times larger in the low gravity specimens as compared with those grown terrestrially. However, the role of convection in determining the dendrite tip radius still remains unanswered. The relationship due to Hunt<sup>[12]</sup> would indicate that at least for a diffusive transport, decrease in the primary arm spacings would be accompanied by a reduction in the tip radii. Since convection decreases the primary arm spacings, one would expect a corresponding decrease in the tip radius. During free growth of dendrites, it is well established that convection does reduce the dendrite tip radius.<sup>[19]</sup> However, during constrained growth, the influence of convection on the tip radius has not been studied. Experiments are currently in progress to determine this.

## V. CONCLUSIONS

In this study, we have examined the macrosegregation resulting from the thermosolutal convection in the interdendritic melt during steady-state columnar growth of lead dendrites in hypoeutectic Pb-Sn alloys, in a positive thermal gradient. The following conclusions can be drawn.

1. Directional solidification of hypoeutectic Pb-Sn alloys, with the melt on top and the solid below, results in gravity induced thermosolutal convection in the mushy zone. This produces macrosegregation along the length of the directionally solidified specimen. The extent of macrosegregation increases with increasing primary dendrite spacings for a constant mushy zone length. For constant primary dendrite spacings, the macrosegregation decreases with increasing mushy zone length.
2. The interdendritic thermosolutal convection is significant only within about 30 pct of the mushy zone length, near the dendrite tips.
3. The primary dendrite spacings should be used as the characteristic length scale in defining the solutal Rayleigh number during columnar dendritic growth. This yields the expected behavior, i.e., increasing Rayleigh number resulting in more intense convection and causing more macrosegregation.

4. Primary dendrite spacings show a systematic decrease with increasing convection. However, the convection in the interdendritic mushy zone has significantly more influence on the spacings as compared to that in the overlying melt, immediately ahead of the dendrite tips.

## ACKNOWLEDGMENTS

This research was supported by a grant from the Microgravity Science and Applications Division of NASA. Appreciation is expressed to Thomas K. Glasgow, Chief, Processing Science and Technology Branch, for supporting this research at the NASA-Lewis Research Center. Help from Bruce Rosenthal, Christopher Palda, and Jerry Loveland is gratefully acknowledged.

## REFERENCES

1. S.N. Tewari and R. Shah: *Metall. Trans. A*, 1992, vol. 23A, pp. 3383-92.
2. S.N. Tewari, R. Shah, and M.A. Chopra: *Metall. Trans. A*, 1993, vol. 24A, pp. 1661-69.
3. S.N. Tewari, R. Shah, and H. Song: *Metall. Trans. A*, 1994, vol. 25A, pp. 1535-44.
4. S.N. Tewari and M.A. Chopra: *Metall. Trans. A*, 1991, vol. 22A, pp. 2467-74.
5. *JAVA*, Jandell Scientific Corporation, 65 Koch Road, Corte Madera, CA 94925. (Our use of the *JAVA* image processing program does not necessarily endorse the use of this product.)
6. J.R. Sazarin and A. Hellawell: *Metall. Trans. A*, 1988, vol. 19A, pp. 1861-71.
7. J.A. Burton, R.C. Prim, and W.P. Slichter: *J. Chem. Phys.*, 1953, vol. 21, pp. 1987-91.
8. D. Camel and J.J. Favier: *J. Cryst. Growth*, 1984, vol. 67, pp. 42-56 and 57-67.
9. J.C. Heinrich, S. Felicelli, P. Nandapurkar, and D.R. Poirier: *Metall. Trans. B*, 1989, vol. 20B, pp. 883-91.
10. G.B. McFadden, R.G. Rehm, S.R. Coriell, W. Chuck, and K.A. Morrish: *Metall. Trans. A*, 1984, vol. 15A, pp. 2125-37.
11. W.M.B. Duval: *Fluid Mechanics Phenomena in Microgravity*, ASME, Fairfield NJ, 1993, AMD-vol. 174/FED-vol. 175.
12. J.D. Hunt: *Solidification Processing and Casting of Metals*, The Metals Society, London, 1979, Book 192, pp. 3-11.
13. V. Laxmanan: *J. Cryst. Growth*, 1986, vol. 83, pp. 573-90.
14. R. Trivedi: *Metall. Trans. A*, 1984, vol. 15A, pp. 977-82.
15. W. Kurz and D.J. Fisher: *Acta Metall.*, 1981, vol. 29, pp. 11-20.
16. J.D. Hunt and D.G. McCartney: *Acta Metall.*, 1987, vol. 35, pp. 89-99.
17. W. Mullins and R.F. Sekerka: *J. Appl. Phys.*, 1964, vol. 35, pp. 444-51.
18. M.D. Dupouy, D. Camel, and J.J. Favier: *Acta Metall. Mater.*, 1992, vol. 40, pp. 1791-99.
19. S.C. Huang and M.E. Glicksman: *Acta Metall.*, 1981, vol. 29, pp. 701-34.